

Emergent Constraints on Regional Cloud Feedbacks

Nicholas J. Lutsko¹

¹Scripps Institution of Oceanography, University of California at San Diego, La Jolla, California.

Max Popp²

²Laboratoire de Météorologie Dynamique, Sorbonne Université, Ecole Normale Supérieure, Ecole Polytechnique, Paris, France.

Robert H. Nazarian³

³Department of Physics, Fairfield University, Fairfield, Connecticut.

Anna Lea Albright²

²Laboratoire de Météorologie Dynamique, Sorbonne Université, Ecole Normale Supérieure, Ecole Polytechnique, Paris, France.

Key Points:

- Low-cloud-based emergent constraints on Equilibrium Climate Sensitivity fail in CMIP6.
- Strong relationships are found between unforced cloud variability and long-term cloud feedbacks in several regions.
- Regional emergent constraints suggest the tropical cloud feedback is likely greater than zero.

Corresponding author: Nicholas Lutsko, nlutsko@ucsd.edu

Abstract

Low-cloud based emergent constraints have the potential to substantially reduce uncertainty in Earth's Equilibrium Climate Sensitivity, but recent work has shown that previously-developed constraints fail in the latest generation of climate models, suggesting that new approaches are needed. Here, we investigate the potential for emergent constraints to reduce uncertainty in regional cloud feedbacks, rather than the global-mean cloud feedback. Strong relationships are found between the monthly/interannual variability of tropical clouds and the tropical net cloud feedback. These relationships are combined with observations to substantially narrow the uncertainty in the tropical cloud feedback and demonstrate that the tropical cloud feedback is likely > 0 . Promising relationships are also found in the 90° - 60° S and 30° - 60° N regions, though these relationships are not robust across model generations and we have not identified the associated physical mechanisms.

1 Introduction

Emergent constraints are a promising tool for constraining uncertainty in Earth's response to increased CO_2 concentrations. The power of emergent constraints lies in relating observable variables with some aspect of the climate system's forced response to substantially narrow the uncertainty in the projected climate response. The canonical example of an emergent constraint was proposed by *Hall and Qu* [2006], who demonstrated a strong correlation across climate models between the amplitude of the seasonal cycle in Northern Hemisphere snow cover and the reduction in Northern Hemisphere snow cover per degree of local warming. This strong correlation has proven to be robust across multiple climate model generations and, when combined with observations of the amplitude of Northern Hemisphere snow cover's seasonal cycle, has allowed tight constraints to be placed on the sensitivity of Northern Hemisphere snow cover to warming [*Qu and Hall, 2014; Thackeray et al., 2018*].

A number of emergent constraints have been proposed for narrowing uncertainty in Earth's Equilibrium Climate Sensitivity (ECS), which can be broadly grouped into three categories: (1) constraints based on historical warming rates (e.g., *Jiménez-de-la Cuesta and Mauritsen* [2019]; *Nijse et al.* [2020]; *Flynn and Mauritsen* [2020]), (2) constraints based on historical temperature variability (e.g., *Cox et al.* [2018]; *Nijse et al.* [2019]),

50 and (3) process-based constraints, often using the variability of subtropical low clouds
51 (e.g., *Qu et al. [2014]* *Sherwood et al. [2014]*; *Brient et al. [2016]*; *Brient and Schneider*
52 *[2016]*; *Siler et al. [2018]*; *Lutsko and Takahashi [2018]*). We focus here on the third type
53 of emergent constraint. Several cloud-based emergent constraints on ECS developed using
54 CMIP5 data proposed that constraining specific cloud processes could substantially reduce
55 uncertainty in ECS; however, when these constraints are re-calculated using CMIP6 data
56 the correlations between the metrics of cloud variability and models' ECS are much lower
57 [*Schlund et al., 2020*]¹. This puts the utility of cloud-based emergent constraints into ques-
58 tion, and suggests that temperature-based constraints may be more fruitful approaches for
59 constraining Earth's ECS.

60 One potential explanation for why cloud-based emergent constraints perform poorly
61 in CMIP6 is that multiple factors are responsible for the spread in ECS across CMIP6
62 models. *Zelinka et al. [2020]* have shown that the high climate sensitivities of many CMIP6
63 models can be attributed in part to extratropical cloud feedbacks, including a less negative
64 cloud feedback over the Southern Ocean, though tropical clouds still play a role. By con-
65 trast, subtropical low clouds are the main source of intermodel spread in climate feedbacks
66 across the CMIP5 models (e.g., *Andrews et al. [2012]*; *Vial et al. [2013]*; *Sherwood et al.*
67 *[2014]*; *Caldwell et al. [2016]*). If multiple cloud-types and regions are responsible for the
68 spread in CMIP6 models' cloud feedback, then a single metric will struggle to constrain
69 the global-mean cloud feedback, and hence will struggle to constrain ECS.

70 These issues suggest that emergent constraints based on cloud variability cannot be
71 used to narrow the spread of ECS among CMIP6 models, but emergent constraints may
72 still be of use in more limited, local contexts. For example, an emergent constraint based
73 on subtropical low cloud variability could be used to constrain the subtropical low cloud
74 feedback, even if it could not be used to constrain the global-mean cloud feedback. Simi-
75 larly, new emergent constraints could be developed for the cloud feedback over the South-
76 ern Ocean. With this motivation, we propose here a new set of emergent constraints on
77 regional cloud feedbacks. To develop these constraints, we have used the same metrics of
78 cloud variability in each region: the regression of deseasonalized monthly surface temper-
79 ature onto deseasonalized monthly Cloud Radiative Effect (CRE, α_m), and the regression

¹ Some cloud-based emergent constraints even perform poorly when applied to CMIP5 models not included in the origi-
nal analysis [*Caldwell et al., 2018*].

80 of annual-mean surface temperature onto annual-mean CRE (α_a). Using the same metrics
81 allows us to simplify the interpretation and methodology, as new metrics do not have to
82 be developed from scratch for each region. Instead, we can standardize the procedure for
83 calculating the emergent constraints and using them to update the probability density func-
84 tions (PDFs) of the regional cloud feedbacks. Using two predictor variables also allows
85 us to check for consistency, as the results of emergent constraints developed with monthly
86 variability should be consistent with the results of emergent constraints developed with
87 interannual variability.

88 Taking this approach, we have investigated the links between α_m and α_a and re-
89 gional cloud feedbacks in the CMIP5 and CMIP6 models. First, we demonstrate that cloud
90 feedbacks in multiple regions contribute to the spread in CMIP6 models' ECS, whereas
91 tropical clouds are the primary source of spread in CMIP5 model's ECS (section 3). This
92 confirms the difficulty of constraining ECS in CMIP6 models using low-cloud based emer-
93 gent constraints and motivates our regional approach. We then evaluate the relationships
94 in each region between α_m and α_a , and the long-term regional cloud feedback (section 4).
95 We do this for both CMIP5 and CMIP6 models to check whether viable emergent con-
96 straints are robust to the choice of models. Finally, in section 5 we use an information-
97 theoretic approach to estimate posterior PDFs of the regional cloud feedbacks in those
98 regions where strong correlations are found between the predictor variables and the re-
99 gional cloud feedbacks. The posterior PDFs account for observational constraints on the
100 regional cloud feedbacks, and our information-theoretic approach ensures that models that
101 are inconsistent with observations have a small influence on the posterior PDFs.

102 **2 Data and Methods**

103 **2.1 Observational data**

104 To estimate the variability of regional cloudiness in observations we have taken 17
105 years of monthly TOA radiative fluxes, spanning the years 2003-2019, from the Clouds
106 and the Earth's Radiant Energy System (CERES-EBAF) dataset. These are matched to
107 surface air temperatures taken from the ERA5 dataset [*Copernicus Climate Change Service*
108 *Climate Data Store (CDS)*, 2017].

2.2 CMIP data

Data are taken from 21 CMIP6 models and 22 CMIP5 models, listed in the Supplementary Material. To estimate the regional cloud feedbacks we take 500 years of data from a pre-industrial control simulation and 150 years of data from an abrupt4XCO₂ simulation with each model. The data include monthly-mean values of surface air temperature, both clear-sky and all-sky TOA fluxes, and vertical pressure velocities at 500hPa (see section 4.3). To estimate α_m and α_a we use linearly de-trended data from a historical simulation with each model, and we repeat our analyses on three non-overlapping 17-year segments for each set of models (1963-1980, 1980-1997, 1997-2014 for CMIP6 and 1954-1971, 1971-1988, 1988-2005 for CMIP5), then average the results.

2.3 Estimating regional cloud feedbacks

We have calculated long-term cloud feedbacks in five regions: 90°S-60°S, 60°S-30°S, 30°S-30°N, 30°N-60°N and 60°N-90°N. In each region, we calculate the net cloud feedback using the Gregory method [Gregory *et al.*, 2004]. First, we linearly detrend the surface temperature and net (longwave plus shortwave) CRE fields, averaged over each region, from the preindustrial control simulations, then subtract these climatological values from the 4XCO₂ data. The long-term regional cloud feedbacks are obtained by regressing the anomalous annual-mean surface temperature onto the anomalous annual-mean net CRE in each region for years 1-150 of the 4XCO₂ simulations.

Gregory regressions are often performed for years 20-150 of 4XCO₂ simulations when estimating a model's ECS, to account for the change in slope as the global-mean radiative feedback evolves [Winton *et al.*, 2010; Geoffroy *et al.*, 2013; Andrews *et al.*, 2015; Armour, 2017]. However, there are no clear changes of slope in the regional Gregory CRE plots (Supplemental Figure 1), and performing the regressions for years 1-150 gives similar values to performing the regressions for years 20-150, though the uncertainties are smaller when more data are used. This is consistent with the change in the net climate feedback being caused by the evolving pattern of the surface temperature response, rather than by changes in the local feedbacks [Armour *et al.*, 2013; Andrews *et al.*, 2015].

We also note that the change in regional CRE per degree of regional warming is not strictly-speaking the "cloud feedback", and does not account for cloud-masking [Soden

139 *et al.*, 2004]. Nevertheless, for ease of presentation we will refer to it as the cloud feed-
 140 back hereafter.

141 **2.4 Calculating posterior PDFs of regional cloud feedbacks**

142 The goal of the emergent constraint methodology is to update the joint multi-model
 143 prior PDF of long-term regional feedbacks P_i , based on the raw model data, using obser-
 144 vational data to obtain a posterior joint multi-model PDF P_f . We do this following the
 145 *Brient and Schneider* [2016] procedure, with one notable difference.

146 The *Brient and Schneider* [2016] procedure uses an information-theoretic distance
 147 measure between the PDFs of the observed and model regression coefficients to assign
 148 a weight w_x to each model x , where $\sum_x w_x = 1$. “Good” models, which have similar
 149 regression coefficients to the observations, are weighted more heavily, and “bad” models,
 150 whose regression coefficients are far from the observations, are given less weight. In this
 151 way, the influence of bad models, which can exert a large leverage on regression slopes, is
 152 minimized.

153 The joint multi-model PDFs P_i and P_f are calculated using Gaussian kernel density
 154 estimates. That is, as a weighted sum of the kernel value K_x associated with each model:

$$P(C) = \sum_x w_x K_x(C), \quad (1)$$

155 where C is the long-term cloud feedback in a given region and

$$K_x(C) = \frac{1}{N} \sum_{z=1,N} \frac{1}{h\sqrt{2\pi}} e^{-0.5\left(\frac{C_x - C_z}{h}\right)^2}. \quad (2)$$

156 N is the number of models, C_x is the regional cloud feedback for model x , C_z is the re-
 157 gional cloud feedback for model z and h is a bandwidth parameter, set to 0.5 in all calcu-
 158 lations, which we found gave a good compromise between smoothing the PDFs and mini-
 159 mizing error. The prior PDF P_i is calculated by assigning each model an identical weight
 160 of $w_x = \frac{1}{N}$, and hence does not distinguish between good or bad models.

161 Calculating the posterior weights requires PDFs for α_m and α_a for each climate
 162 model and for the observational data. We assume in both models and observations that the
 163 PDFs of α_m and α_a are Gaussian, and can be characterized by their mean values and stan-
 164 dard deviations. The mean values of α_m and α_a are given by the regression coefficients of
 165 the monthly or annual regional surface temperature onto the regional CRE. The standard
 166 deviations are estimated by multiplying the standard errors of the linear regressions by the

167 square root of the sample sizes ($\sqrt{204}$ for the monthly data and $\sqrt{17}$ for the annual data).
 168 We note that *Brient and Schneider* [2016] used a bootstrapping procedure to estimate the
 169 standard deviations in their metric of low cloud variability, but this is difficult to use here
 170 because of the small number of samples for the annual-mean data.

171 Together with the mean values of the regression slopes, the standard deviations are
 172 used to generate Gaussian PDFs of α_m and α_a for each model and for the observations.
 173 The model PDFs are denoted by $M_{m,x}$ and $M_{a,x}$ for the monthly and annual variability,
 174 respectively, and the observational PDFs are denoted by O_m and O_a . Note that we calcu-
 175 late three sets of model PDFs, one for each 17-year interval.

Next, we calculate the Kullback-Leibler divergence for each model PDF:

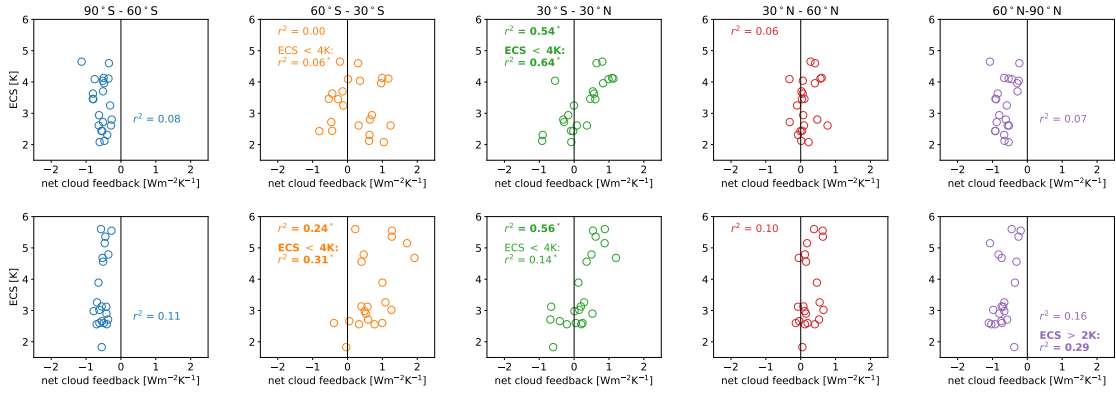
$$\Delta_x = \int O(\alpha) \log \left(\frac{O(\alpha)}{M_x(\alpha)} \right) d\alpha, \quad (3)$$

176 where we have dropped the m and a subscripts for convenience, but note that two sets
 177 of Δ_x values are calculated for each 17-year period. Δ_x is the relative entropy between
 178 O and M_x , and measures how much information is lost if M_x is used to approximate O .
 179 Importantly, this assumes the time-series used to estimate M_x is the same length as the
 180 time-series used to estimate O . The likelihood of model x giving rise to the observed dis-
 181 tribution O is the exponential $l_x = \exp(-\Delta_x)$, so that normalized weights can be calculated
 182 as $w_x = \frac{l_x}{\sum_x l_x}$. Similar to weights in Bayesian model averages, the values of w_x can be in-
 183 terpreted as the posterior probability that model x is the best model for the data according
 184 to the Kullback–Leibler measure [*Brient and Schneider*, 2016].

191 3 Sources of Intermodel Spread in ECS

192 The regional cloud feedbacks, calculated as described in section 2.3, can be used to
 193 quantify the contributions different regions make to the intermodel spread in ECS. For ex-
 194 ample, the top row of Figure 1 demonstrates that in CMIP5 the tropical cloud feedback
 195 is highly correlated with ECS ($r^2 = 0.54$, all ECS values are taken from *Zelinka et al.*
 196 [2020]), while the cloud feedbacks in all other regions are not well correlated with ECS.
 197 Hence the tropical cloud feedback is the main source of uncertainty in CMIP5 models’
 198 ECS.

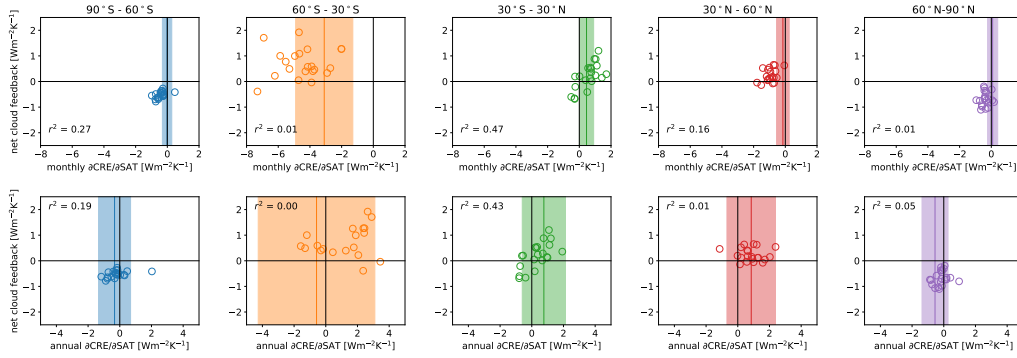
199 By contrast, in CMIP6 the cloud feedbacks in multiple regions are well correlated
 200 with ECS (bottom row of Figure 1; we define a correlation as statistically significant if its



185 **Figure 1.** ECS values of the 22 CMIP5 (top) and 21 CMIP6 (bottom) models, plotted versus the regional
 186 cloud feedbacks in the five regions. r^2 values for correlations between ECS and the regional cloud feedbacks
 187 are written in each panel, with bold values and asterisks denoting correlations with p -values less than 0.05,
 188 which we take as a measure of statistical significance. The panels for 60°-30°S and 30°S-30°N also show r^2
 189 values for correlations over models with ECS<4K, and the 60°-90°N panels show r^2 values for correlations
 190 over models with ECS>2K.

201 associated p -value is less than 0.05). The correlation between the tropical cloud feedback
 202 and ECS again has a high r^2 value of 0.56, but the correlation between the cloud feedback
 203 in the Southern Hemisphere mid-latitudes and ECS is also statistically significant ($r^2 =$
 204 0.24). Interestingly, the Arctic cloud feedback shows a strong relationship with ECS when
 205 an outlier model (INM-CM4-8) which has an ECS of less than 2K, is ignored ($r^2 = 0.29$).

206 To investigate these relationships further, we have divided the CMIP6 models into
 207 high sensitivity (ECS > 4K) and low sensitivity (ECS < 4K) models. Repeating the cor-
 208 relations, we find that the tropical cloud feedback is not well correlated with the low sen-
 209 sitivity models' ECS ($r^2 = 0.14$, Figure 1), while the correlation with the Southern Hemi-
 210 sphere mid-latitude cloud feedback is stronger for the low sensitivity models ($r^2 = 0.31$;
 211 the tropical and Southern Hemisphere mid-latitude clouds feedbacks are poorly correlated
 212 among the low ECS models). Thus in CMIP6, tropical cloud feedbacks can distinguish
 213 very high climate sensitivity models from lower sensitivity models, but cannot distinguish
 214 between a 2K and a 4K model. Conversely, the Southern Hemisphere mid-latitudes can
 215 distinguish between 2K and 4K models, but are less useful for evaluating high climate
 216 sensitivities.



225 **Figure 2.** Mean values of α_m (top row) and α_a (bottom row) in the five geographic regions plotted versus
 226 the net cloud feedback in each region for 21 CMIP6 models. Only the regression coefficients calculated using
 227 the last 17 years of each historical simulation are shown. The shaded regions show 5-95% confidence inter-
 228 vals for estimates of the linear regressions from CERES-EBAF data, with the solid lines showing the mean of
 229 the observational regression estimates.

217 These results demonstrate why low-cloud based emergent constraints perform poorly
 218 in CMIP6: a model with a large positive tropical cloud feedback likely has a high ECS,
 219 but a model with a negative tropical cloud feedback, or a tropical cloud feedback close to
 220 zero, could have an ECS of 2K or 4K. In contrast, dividing the CMIP5 models into high
 221 and low sensitivity models still gives robust relationships between tropical clouds and ECS
 222 (Figure 1).

223 4 Evaluating Regional Emergent Constraints

224 4.1 Robust relationships

230 There are several robust relationships between the metrics of variability α_m and
 231 α_a and the regional cloud feedbacks. Most notably, the regression coefficients for both
 232 monthly and interannual variability in the tropics (30°S to 30°N) are highly correlated
 233 with the tropical cloud feedback in both sets of models (Table 1, Figure 2, Supplemental
 234 Figure S2). Other notable relationships are seen for the 90°-60°S region in CMIP6, and
 235 the 30°-60°N region in CMIP5. In both cases, two out of the three correlations are statis-
 236 tically significant, while the p -value for the third correlation is just over the 0.05 thresh-
 237 old.

238 **Table 1.** r^2 values for correlations across the models between α_m/α_a in each region and the long term
 239 regional cloud feedbacks. Columns 2 and 3 show three sets of values, one for each 17-year period of the
 240 historical simulations. Columns 4 and 5 show correlations when α_m and α_a are estimated using the last 50
 241 years of each simulation. Correlations with a p -value less than 0.05, which we use as a measure of statistical
 242 significance, are in bold.

Region	17-year α_m	17-year α_a	50-year α_m	50-year α_a
CMIP6				
90°S-60°S	0.25/0.19/0.27	0.12/0.10/0.19	0.23	0.19
60°S-30°S	0.08/0.08/0.01	0.08/0.08/0.00	0.31	0.34
30°S-30°N	0.37/0.60/0.47	0.28/0.50/0.43	0.44	0.59
30°N-60°N	0.11/0.11/0.16	0.04/ 0.21 /0.01	0.20	0.08
60°N-90°N	0.05/0.07/0.01	0.03/0.10/0.05	0.0	0.02
CMIP5				
90°S-60°S	0.0/0.0/0.0	0.18/0.02/0.07	0.08	0.09
60°S-30°S	0.0/0.0/0.01	0.03/0.18/ 0.29	0.09	0.33
30°S-30°N	0.47/0.35/0.51	0.59/0.42/0.36	0.60	0.60
30°N-60°N	0.15/ 0.27/0.26	0.03/ 0.28 /0.17	0.35	0.26
60°N-90°N	0.02/0.0/0.0	0.04/0.08/0.0	0.03	0.01
Joint				
90°S-60°S	0.03/0.01/0.02	0.09/0.03/0.09	0.11	0.08
60°S-30°S	0.01/0.00/0.00	0.13/0.01/ 0.13	0.13	0.38
30°S-30°N	0.41/0.39/0.42	0.46/0.42/0.38	0.49	0.59
30°N-60°N	0.15/0.23/0.23	0.00/ 0.21 /0.06	0.28	0.19
60°N-90°N	0.01/0.03/0.00	0.02/0.1/0.00	0.02	0.03

243 The observed α_m values for the 30°-60°N region are outside the intermodel spread
 244 in CMIP5 (Supplemental Figure 2), implying that all models struggle to simulate cloud
 245 variability in this region and that we should be cautious about using this relationship to
 246 update the regional cloud feedback. Nevertheless, the observations and implied relation-
 247 ship do suggest that the regional cloud feedback in this region is more positive than is
 248 simulated by the models. For the 90°-60°S region, there is one outlier model (CNRM-
 249 CM6-1) which is far from the observations and from the other models. Disregarding this
 250 model increases the correlation between α_m and the regional cloud feedback slightly (not
 251 shown), but our methodology will anyways assign a small weight to this model when cal-
 252 culating the posterior PDF.

253 As another test of the robustness of these relationships, we have taken correlations
 254 across the joint ensemble of CMIP5 and CMIP6 data. The r^2 values of these correlations
 255 are consistent with the findings from the individual ensembles (third set of rows in Table
 256 1), with the exception of the 90°-60°S region, for which the high correlations found in
 257 CMIP6 disappear in the joint ensemble. This is not surprising, since the correlations in
 258 this region are very low in CMIP5, but suggest further caution.

259 4.2 Using longer time-series

260 17 years of observational data is a short record with which to search for robust
 261 correlations, but the methodology used to calculate the posterior PDFs requires that the
 262 model and observational time-series have the same lengths. To investigate whether more
 263 robust relationships emerge with longer datasets, we have also calculated the variability
 264 coefficients α_m and α_a using the last 50 years of the historical simulations (1964 – 2014
 265 in CMIP6 and 1955 – 2005 in CMIP5). Correlating these new coefficients with the re-
 266 gional cloud feedbacks gives stronger relationships than the 17 year coefficients (Table 1,
 267 Supplemental Figures S3 and S4), with statistically significant relationships between α_m
 268 and/or α_a and the cloud feedbacks in all regions except for the high northern latitudes
 269 (60°-90°N).

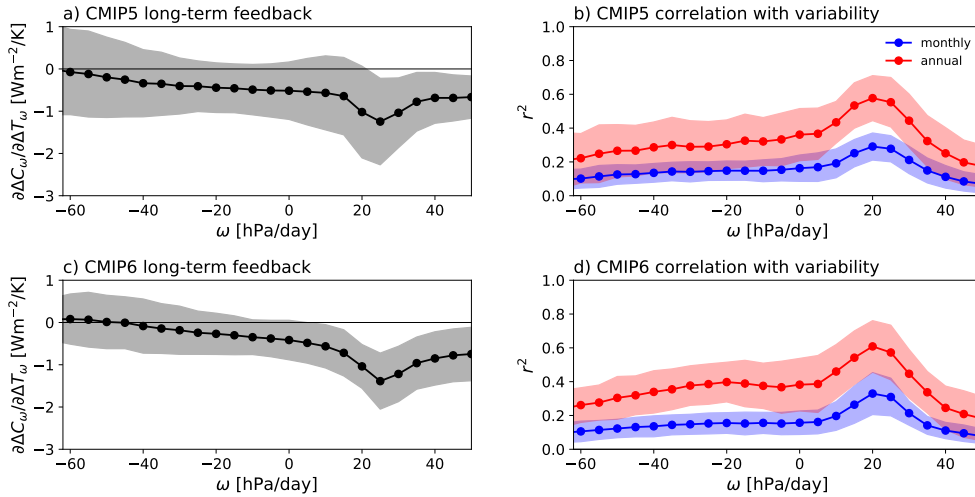
270 The strong correlations for the 60°S-30°S region² are of particular interest, as the
 271 Southern Hemisphere mid-latitudes have been identified as one of the causes of the high

² The low correlation for the CMIP5 α_m s is due to an outlier model. See Supplemental Figure S4.

272 climate sensitivities in certain CMIP6 models [Zelinka *et al.*, 2020]. The calculations in
273 section 3 further demonstrate the importance of this region for the spread in ECS among
274 CMIP6 models. However, our previous calculations demonstrated that the relationships
275 between monthly/interannual variability of surface temperature and CRE in the South-
276 ern Hemisphere mid-latitudes cannot be robustly identified from 17 years of observational
277 data, so we cannot use observations and the methodology described in section 2.4 to con-
278 strain the cloud feedback in this region. Moreover, the large observational uncertainty in
279 this region suggests that emergent relationships are unlikely to be of practical use for con-
280 straining the 60°S-30°S cloud feedback in the near future, even with other methodologies.

281 **4.3 Explaining the high correlations in the tropics**

282 Emergent constraints are sometimes criticised as being the result of data mining
283 (Caldwell *et al.* [2014, 2018]; Hall *et al.* [2019]), with no physical basis for the proposed
284 relationships. Here, our starting assumption is that the intermodel spread in cloud physics
285 is time-scale invariant (note that we are not assuming the cloud physics itself is invariant,
286 but that the causes of intermodel spread are invariant). This is reasonable in the tropics,
287 where previous emergent constraints have linked the variability of specific tropical and
288 subtropical clouds to the net cloud feedback (e.g., Zhai *et al.* [2015]; Brient and Schneider
289 [2016]; Lutsko [2018]). Moreover, our results demonstrate that the unforced variability of
290 the tropical-mean cloud feedback, which includes contributions from all tropical cloud-
291 types, is related to the forced tropical-mean cloud feedback. This suggests that the same
292 clouds are responsible for intermodel spread in the variability and in the cloud feedback.
293 To confirm this, we have binned the net CRE and surface temperature values based on
294 the corresponding pressure velocities at 500hPa (ω_{500}), which is an effective method for
295 separating out different cloud regimes in the tropics, where high clouds tend to form in
296 regions of large-scale ascent and low clouds tend to form in regions of large-scale descent
297 [Bony *et al.*, 2004; Bony and Dufresne, 2005]. The left panels of Figure 3 show the trop-
298 ical cloud feedback in each ω_{500} bin, and the right panels show correlations between the
299 monthly/annual variability of tropical net CRE in each ω_{500} bin and the monthly/annual
300 variability of tropical-mean net CRE over the historical simulations. Clouds in regimes
301 of weak-to-moderate descent clearly make the largest contributions to the tropical cloud
302 feedback (left panels) and also have the highest correlations with the tropical-mean CRE
303 (right panels), consistent with the large statistical weight of these subtropical low clouds

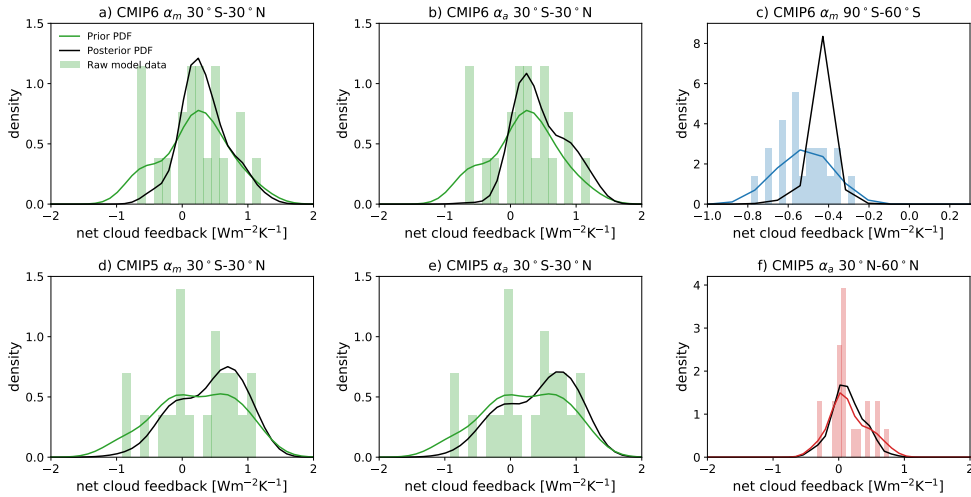


308 **Figure 3.** a) Long-term CMIP5 tropical cloud feedback in ω_{500} bins, calculated following *Bony and*
 309 *Dufresne* [2005] by dividing the long-term tropical net CRE trend in each 5hPa bin over years 1-150 of
 310 abrupt4XCO₂ simulations by the long-term surface temperature trend in each bin. The black markers show
 311 the multi-model mean values and the gray shading shows ± 1 standard deviation. b) r^2 values for correla-
 312 tions in the CMIP5 models between the monthly (blue) and annual-mean (red) CRE in each 5hPa bin and the
 313 tropical-mean CRE over the final 50 years of the historical simulations. The markers show the multi-model
 314 mean values and the shadings show ± 1 standard deviation. c) Same as panel a but for CMIP6 models. d)
 315 Same as panel b but for CMIP6 models.

304 [*Bony and Dufresne, 2005*]. Hence in both sets of models, our simple metrics of tropical
 305 cloud variability mostly reflect the contributions of low clouds to monthly and interannual
 306 cloud variability, and these clouds are also the main source of uncertainty in the long-term
 307 tropical cloud feedback.

316 These results are consistent with *Lutsko* [2018], who showed that (in models) the
 317 variations in tropical CRE during the ENSO cycle are mostly due to low clouds, with high
 318 and mid-level clouds making minor contributions. So, while high and mid-level clouds
 319 may show substantial differences in spatial organization on monthly, annual and ENSO
 320 time-scales, they make relatively small contributions to the variability of the tropical-mean
 321 radiation budget.

334 The physical mechanisms linking variability in other regions and the regional cloud
 335 feedbacks are less clear, and may be more difficult to identify, given the larger seasonal



322 **Figure 4.** a) Prior and posterior PDFs of the tropical cloud feedback in CMIP6. The green bars show the
 323 raw model distribution of tropical cloud feedbacks and the green curves show the prior PDFs estimated using
 324 Gaussian kernel estimates. The black curves show the posterior PDFs obtained using monthly variability,
 325 following the procedure described in section 2.4. b) Same as panel a but the posterior PDF is obtained using
 326 interannual variability. c) Prior and posterior PDFs of the cloud feedback in the 90°-60°S region in CMIP6.
 327 The blue bars show the raw model distribution of regional cloud feedbacks and the blue curves show the prior
 328 PDFs estimated using Gaussian kernel estimates. The black curves show the posterior PDFs obtained using
 329 monthly variability, following the procedure described in section 2.4. d) Same as panel a but for the CMIP5
 330 models. e) Same as panel b but for CMIP5 data. f) Prior and posterior PDFs of the cloud feedback in the
 331 30°-60°N region in CMIP5. The red bars show the raw model distribution of regional cloud feedbacks and
 332 the red curves show the prior PDFs estimated using Gaussian kernel estimates. The black curves show the
 333 posterior PDFs obtained using monthly variability, following the procedure described in section 2.4.

336 cycles at higher latitudes. We leave it to future work to identify the mechanisms, but note
 337 again that the results for 90°-60°S and 30°-60°N should be taken with caution until physi-
 338 cal mechanisms can be identified.

339 5 Constraining Regional Cloud Feedbacks

340 Section 4 established the existence of robust relationships between the variability
 341 of tropical cloudiness on monthly and interannual time-scales, and the long-term tropi-
 342 cal cloud feedback. Statistically significant relationships were also found in the CMIP6

343 models between the monthly variability of cloudiness and the regional cloud feedback at
 344 90° - 60° S and in CMIP5 between the monthly variability of cloudiness and the regional
 345 cloud feedback at 30° - 60° N, though these relationships are less robust, particularly since
 346 they are only found in one generation of models. Using the procedure described in section
 347 2.4, we have estimated posterior PDFs for the cloud feedbacks in the three regions, with
 348 the results shown in Figure 4 (the posterior weights are listed in Supplemental Tables S1
 349 and S2).

350 In both sets of models, the monthly and interannual results for the tropics are re-
 351 markably similar. Panels a and d show that using α_m and α_a with the CMIP6 data re-
 352 sults in very similar posterior tropical cloud feedback PDFs, while panels b and e show
 353 the same for the CMIP5 data. In both sets of models, and for both α_m and α_a , the poste-
 354 rior PDFs are weighted more heavily towards positive values than the prior PDFs. This is
 355 particularly true in the CMIP6 models, where the posterior PDF is considerably narrower:
 356 in CMIP6 the 5-95 percentile confidence intervals go from $-0.65 - 1.26 \text{ Wm}^{-2} / \text{K}$ in the
 357 prior PDF to $0.06 - 1.37 \text{ Wm}^{-2} / \text{K}$ in the posterior PDF obtained using annual data or
 358 $-0.09 - 1.18 \text{ Wm}^{-2} / \text{K}$ in the posterior PDF obtained using monthly data. In CMIP5 the
 359 5-95 percentile confidence intervals go from $-0.77 - 1.38 \text{ Wm}^{-2} / \text{K}$ in the prior PDF to
 360 $-0.39 - 1.44 \text{ Wm}^{-2} / \text{K}$ in the posterior PDF obtained using annual data or $-0.32 - 1.40$
 361 $\text{Wm}^{-2} / \text{K}$ in the posterior PDF obtained using monthly data. The shifts of the posterior
 362 PDFs towards more positive values are consistent with other lines of evidence pointing to
 363 a positive tropical cloud feedback [Myers and Norris, 2016; Klein et al., 2018; Scott et al.,
 364 2020; Sherwood et al., 2020]. We have not investigated why the posterior PDFs are nar-
 365 rower when using the CMIP6 data than when using the CMIP5 data, but note that the
 366 distribution of tropical cloud feedbacks in CMIP5 is more bimodal than in CMIP6, with
 367 maxima close to $0 \text{ Wm}^{-2} / \text{K}$ and near $0.8 \text{ Wm}^{-2} / \text{K}$. The posterior PDFs retain this bimodal-
 368 ity, but with more weight on the maximum at $0.8 \text{ Wm}^{-2} / \text{K}$.

369 For the other two regions, the posterior PDF for 90° S- 60° S has a strong peak at
 370 around $-0.5 \text{ Wm}^{-2} / \text{K}$ and is substantially narrower than the prior; while the posterior PDF
 371 for 30° - 60° N is only slightly narrower than the prior. Thus an emergent constraint based
 372 on the monthly variability at 90° S- 60° S has the potential to strongly constrain the cloud
 373 feedback in this region, though more work is needed to confirm this result. It will be dif-
 374 ficult to use emergent constraints for the feedback at 30° - 60° N since the models do a poor
 375 job at reproducing the variability in this region.

6 Conclusion

The results presented here demonstrate that both the monthly and the interannual variability of cloudiness in the tropics can be used to constrain the tropical cloud feedback, with CMIP5 and CMIP6 results suggesting that the tropical cloud feedback is on the higher end of the intermodel range, and likely greater than zero. This is consistent with recent work using cloud-controlling factors to constrain the tropical cloud feedback [Myers and Norris, 2016; Klein et al., 2018; Scott et al., 2020]. At higher latitudes, we have tentatively shown that emergent constraints can be applied to the regional cloud feedbacks at 90°-60°S and 30°-60°N; with the variability in the 90°-60°S region showing particular promise as the basis for an emergent constraint. However, the high correlations between the monthly variability and cloud feedbacks in these regions are not robust across both generations of models, and we have not identified the physical mechanisms responsible for the relationships.

Another factor which limits the effectiveness of cloud-based emergent constraints is the relatively short length of the satellite record (~17 years). Using 50 years of model data, we have found statistically significant relationships between cloud variability and regional cloud feedbacks in all regions except for 60°-90°N. This hints that the cloud feedback in the Southern Hemisphere mid-latitudes (60°-30°S), a key region for the high climate sensitivities of CMIP6 models, could be constrained using the local unforced variability. Unfortunately, our metrics of variability have the highest observational uncertainty in this region, and more data will be needed before emergent constraints can be used to constrain the cloud feedback in the Southern Hemisphere mid-latitudes. Other approaches, for example which focus on the simulation of specific cloud properties (e.g., Ceppi et al. [2016]), may be more successful moving forward.

Cloud-based emergent constraints developed in CMIP5 consistently indicated ECS is on the higher end of the intermodel range (3-4°C, see Bretherton and Caldwell [2020]), in contrast to recent temperature-based emergent constraints which generally indicate lower ECS values (2-3°C, e.g., Cox et al. [2018]; Jiménez-de-la Cuesta and Mauritsen [2019]). Reconciling these two opposing lines of evidence is of crucial importance for improving our confidence in ECS estimates. While the failure of cloud-based emergent constraints in CMIP6 does not rule out the possibility of high ECS values, it does suggest that a more

407 nuanced approach, moving cloud-type by cloud-type and region-by-region, will be required
408 to reduce uncertainty in Earth's cloud feedback.

409 **Acknowledgments**

410 We thank Joel Norris for helpful discussions and comments on an earlier version of this
411 manuscript. N.J.L. was supported by the NOAA Climate Program Office's Modeling,
412 Analysis, Predictions, and Projections program through grant NA20OAR4310387. M. P.
413 acknowledges funding from the Centre National D' études Spatiales (CNES). The CMIP5
414 and CMIP6 data are publicly available at: <https://esgf-node.llnl.gov/projects/esgf-llnl/>, the
415 ERA5 data are publicly available at: [https://www.ecmwf.int/en/forecasts/datasets/reanalysis-](https://www.ecmwf.int/en/forecasts/datasets/reanalysis-datasets/era5)
416 [datasets/era5](https://www.ecmwf.int/en/forecasts/datasets/reanalysis-datasets/era5) and the CERES-EBAF data are publicly available from: <https://ceres.larc.nasa.gov/data/>.
417 Jupyter notebooks with the analysis and processing scripts are available at *Lutsko* [2021].

418 **References**

- 419 Andrews, T., J. M. Gregory, M. J. Webb, and K. E. Taylor (2012), Forcing, feedbacks and
420 climate sensitivity in cmip5 coupled atmosphere-ocean climate models, *Geophysical*
421 *Research Letters*, 39(9), 109712.
- 422 Andrews, T., J. M. Gregory, and M. J. Webb (2015), The dependence of radiative forcing
423 and feedback on evolving patterns of surface temperature change in climate models.,
424 *Journal of Climate*, 28(2), 1630–1648.
- 425 Armour, K. C. (2017), Energy budget constraints on climate sensitivity in light
426 of inconstant climate feedbacks, *Nature Climate Change*, 7(5), 331–335, doi:
427 10.1038/nclimate3278, number: 5 Publisher: Nature Publishing Group.
- 428 Armour, K. C., C. M. Bitz, and G. H. Roe (2013), Time-Varying Climate Sensitivity from
429 Regional Feedbacks, *Journal of Climate*, 26(13), 4518–4534, doi:10.1175/JCLI-D-12-
430 00544.1.
- 431 Bony, S., and J. L. Dufresne (2005), Marine boundary layer clouds at the heart of tropical
432 cloud feedback uncertainties in climate models., *Geophysical Research Letters*, 32(6),
433 L20,806.
- 434 Bony, S., J.-L. Dufresne, H. Le Treut, J.-J. Morcrette, and C. Senior (2004), On dynamic
435 and thermodynamic components of cloud changes, *Climate Dynamics*, 22(2), 71–86,
436 doi:10.1007/s00382-003-0369-6.

- 437 Bretherton, C. S., and P. M. Caldwell (2020), Combining Emergent Constraints for Cli-
 438 mate Sensitivity, *Journal of Climate*, *33*(17), 7413–7430, doi:10.1175/JCLI-D-19-
 439 0911.1, publisher: American Meteorological Society Section: Journal of Climate.
- 440 Brient, F., and T. Schneider (2016), Constraints on Climate Sensitivity from Space-Based
 441 Measurements of Low-Cloud Reflection, *Journal of Climate*, *29*(16), 5821–5835.
- 442 Brient, F., T. Schneider, Z. Tan, S. Bony, X. Qu, and A. Hall (2016), Shallowness of trop-
 443 ical low clouds as a predictor of climate models' response to warming, *Climate Dynam-*
 444 *ics*, *47*(1-2), 433–449.
- 445 Caldwell, P. M., C. S. Bretherton, M. D. Zelinka, S. A. Klein, B. D. San-
 446 ter, and B. M. Sanderson (2014), Statistical significance of climate sen-
 447 sitivity predictors obtained by data mining, *Geophysical Research Let-*
 448 *ters*, *41*(5), 1803–1808, doi:<https://doi.org/10.1002/2014GL059205>, _eprint:
 449 <https://agupubs.onlinelibrary.wiley.com/doi/pdf/10.1002/2014GL059205>.
- 450 Caldwell, P. M., M. D. Zelinka, K. E. Taylor, and K. Marvel (2016), Quantifying the
 451 Sources of Intermodel Spread in Equilibrium Climate Sensitivity, *Journal of Climate*,
 452 *29*(2), 513–524, doi:10.1175/JCLI-D-15-0352.1, publisher: American Meteorological
 453 Society Section: Journal of Climate.
- 454 Caldwell, P. M., M. D. Zelinka, and S. A. Klein (2018), Evaluating Emergent Con-
 455 straints on Equilibrium Climate Sensitivity, *Journal of Climate*, *31*(10), 3921–3942,
 456 doi:10.1175/JCLI-D-17-0631.1, publisher: American Meteorological Society Section:
 457 Journal of Climate.
- 458 Ceppi, P., D. T. McCoy, and D. L. Hartmann (2016), Observational evidence for a nega-
 459 tive shortwave cloud feedback in middle to high latitudes, *Geophysical Research Letters*,
 460 *43*(3), 1331–1339, doi:10.1002/2015GL067499.
- 461 Copernicus Climate Change Service Climate Data Store (CDS) (2017), Coper-
 462 nicus Climate Change Service (c3s) (2017): ERA5: Fifth generation of
 463 ECMWF atmospheric reanalyses of the global climate, accessed 02 March 2018,
 464 <https://cds.climate.copernicus.eu/cdsapp!/home>.
- 465 Cox, P. M., C. Huntingford, and M. S. Williamson (2018), Emergent constraint on equi-
 466 librium climate sensitivity from global temperature variability, *Nature*, *553*(7688), 319–
 467 322, doi:10.1038/nature25450, number: 7688 Publisher: Nature Publishing Group.
- 468 Flynn, C. M., and T. Mauritsen (2020), On the climate sensitivity and historical warm-
 469 ing evolution in recent coupled model ensembles, *Atmospheric Chemistry and Physics*,

- 470 20(13), 7829–7842, doi:10.5194/acp-20-7829-2020.
- 471 Geoffroy, O., D. Saint-Martin, G. Bellon, A. Voldoire, D. J. L. Olivie, and S. Tyteca
472 (2013), Transient climate response in a two-layer energy-balance model. part ii: Rep-
473 resentation of the efficacy of deep-ocean heat uptake and validation for cmip5 aogcms,
474 *Journal of Climate*, 26(6), 1859–1876.
- 475 Gregory, J. M., W. J. Ingram, M. A. Palmer, G. S. Jones, P. A. Stott, R. B. Thorpe, J. A.
476 Lowe, T. C. Johns, and K. D. Williams (2004), A new method for diagnosing radiative
477 forcing and climate sensitivity, *Geophysical Research Letters*, 31, L03,205.
- 478 Hall, A., and X. Qu (2006), Using the current seasonal cycle to constrain snow
479 albedo feedback in future climate change., *Geophysical Research Letters*, 33(23),
480 2006GL03502.
- 481 Hall, A., P. Cox, C. Huntingford, and S. Klein (2019), Progressing emergent constraints on
482 future climate change, *Nature Climate Change*, 9(4), 269–278, doi:10.1038/s41558-019-
483 0436-6, number: 4 Publisher: Nature Publishing Group.
- 484 Jiménez-de-la Cuesta, D., and T. Mauritsen (2019), Emergent constraints on Earth’s tran-
485 sient and equilibrium response to doubled CO₂ from post-1970s global warming, *Na-
486 ture Geoscience*, 12(11), 902–905, doi:10.1038/s41561-019-0463-y, number: 11 Pub-
487 lisher: Nature Publishing Group.
- Klein, S. A., A. Hall, J. R. Norris, and R. Pincus (2018), Low-Cloud Feedbacks from
Cloud-Controlling Factors: A Review, in *Shallow Clouds, Water Vapor, Circulation, and
Climate Sensitivity*, edited by R. Pincus, D. Winker, S. Bony, and B. Stevens, pp. 135–
157, Springer International Publishing, Cham, doi:10.1007/978-3-319-77273-8_7.
- 488 Lutsko, N. J. (2018), The relationship between cloud radiative effect and surface temperature
489 variability at enso frequencies in cmip5 models., *Geophysical Research Letters*, 45, 10,599
490 – 10,608.
- Lutsko, N. J. (2021), nicklutsko/regional_emergent_constraints :
Firstrelease(versionv1.0.0)., doi : [http : //doi.org/10.5281/zenodo.4531393](http://doi.org/10.5281/zenodo.4531393).
- 491 Lutsko, N. J., and K. Takahashi (2018), What can the internal variability of cmip5 models
492 tell us about their climate sensitivity?, *Journal of Climate*, 31, 5051 – 5069.
- 493 Myers, T. A., and J. R. Norris (2016), Reducing the uncertainty in
494 subtropical cloud feedback, *Geophysical Research Letters*, 43(5),
495 2144–2148, doi:<https://doi.org/10.1002/2015GL067416>, _eprint:
496 <https://agupubs.onlinelibrary.wiley.com/doi/pdf/10.1002/2015GL067416>.

- 497 Nijssen, F. J. M. M., P. M. Cox, C. Huntingford, and M. S. Williamson (2019), Decadal
 498 global temperature variability increases strongly with climate sensitivity, *Nature Climate*
 499 *Change*, 9(8), 598–601, doi:10.1038/s41558-019-0527-4, number: 8 Publisher: Nature
 500 Publishing Group.
- 501 Nijssen, F. J. M. M., P. M. Cox, and M. S. Williamson (2020), Emergent constraints on tran-
 502 sient climate response (TCR) and equilibrium climate sensitivity (ECS) from historical
 503 warming in CMIP5 and CMIP6 models, *Earth System Dynamics*, 11(3), 737–750, doi:
 504 10.5194/esd-11-737-2020.
- 505 Qu, X., and A. Hall (2014), On the persistent spread in snow-albedo feedback, *Climate Dy-*
 506 *namics*, 42(1), 69–81, doi:10.1007/s00382-013-1774-0.
- 507 Qu, X., A. Hall, S. A. Klein, and P. M. Caldwell (2014), On the spread of changes in ma-
 508 rine low cloud cover in climate model simulations of the 21st century, *Climate Dynamics*,
 509 42(9), 2603–2626, doi:10.1007/s00382-013-1945-z.
- 510 Schlund, M., A. Lauer, P. Gentine, S. C. Sherwood, and V. Eyring (2020), Emergent con-
 511 straints on equilibrium climate sensitivity in CMIP5: do they hold for CMIP6?, *Earth Sys-*
 512 *tem Dynamics*, 11(4), 1233–1258, doi:10.5194/esd-11-1233-2020.
- 513 Scott, R. C., T. A. Myers, J. R. Norris, M. D. Zelinka, S. A. Klein, M. Sun, and D. R.
 514 Doelling (2020), Observed Sensitivity of Low-Cloud Radiative Effects to Meteorologi-
 515 cal Perturbations over the Global Oceans, *Journal of Climate*, 33(18), 7717–7734, doi:
 516 10.1175/JCLI-D-19-1028.1, publisher: American Meteorological Society Section: Journal
 517 of Climate.
- 518 Sherwood, S. C., S. Bony, and J.-L. Dufresne (2014), Spread in model climate sensitivity
 519 traced to atmospheric convective mixing, *Nature*, 505, 37–42.
- 520 Sherwood, S. C., M. J. Webb, J. D. Annan, K. C. Armour, P. M. Forster, J. C. Hargreaves,
 521 G. Hegerl, S. A. Klein, K. D. Marvel, E. J. Rohling, M. Watanabe, T. Andrews, P. Bracon-
 522 not, C. S. Bretherton, G. L. Foster, Z. Hausfather, A. S. v. d. Heydt, R. Knutti, T. Mau-
 523 ritsen, J. R. Norris, C. Proistosescu, M. Rugenstein, G. A. Schmidt, K. B. Tokarska, and
 524 M. D. Zelinka (2020), An assessment of Earth’s climate sensitivity using multiple lines of
 525 evidence, *Reviews of Geophysics*, n/a(n/a), e2019RG000,678.
- 526 Siler, N., S. Po-Chedley, and C. S. Bretherton (2018), Variability in modeled cloud feedback
 527 tied to differences in the climatological spatial pattern of clouds, *Climate Dynamics*, 50(3),
 528 1209–1220, doi:10.1007/s00382-017-3673-2.

- 529 Soden, B. J., A. J. Broccoli, and R. S. Hemler (2004), On the Use of Cloud Forcing to
530 Estimate Cloud Feedback, *Journal of Climate*, 17(19), 3661–3665, doi:10.1175/1520-
531 0442(2004)017<3661:OTUOCF>2.0.CO;2, publisher: American Meteorological Society
532 Section: Journal of Climate.
- 533 Thackeray, C. W., X. Qu, and A. Hall (2018), Why Do Models Pro-
534 duce Spread in Snow Albedo Feedback?, *Geophysical Research Letters*,
535 45(12), 6223–6231, doi:<https://doi.org/10.1029/2018GL078493>, _eprint:
536 <https://agupubs.onlinelibrary.wiley.com/doi/pdf/10.1029/2018GL078493>.
- 537 Vial, J., J.-L. Dufresne, and S. Bony (2013), On the interpretation of inter-model spread in
538 cmip5 climate sensitivity estimates., *Climate Dynamics*, 41(1), 3339–3362.
- 539 Winton, M., K. Takahashi, and I. M. Held (2010), Importance of ocean heat uptake efficacy
540 to transient climate change, *Journal of Climate*, 23(6), 2333–2344.
- 541 Zelinka, M. D., T. A. Myers, D. T. McCoy, S. Po-Chedley, P. M. Caldwell, P. Ceppi, S. A.
542 Klein, and K. E. Taylor (2020), Causes of Higher Climate Sensitivity in CMIP6 Models,
543 *Geophysical Research Letters*, 47(1), e2019GL085,782.
- 544 Zhai, C., J. H. Jiang, and H. Su (2015), Long-term cloud change imprinted in sea-
545 sonal cloud variation: More evidence of high climate sensitivity, *Geophysical Re-*
546 *search Letters*, 42(20), 8729–8737, doi:<https://doi.org/10.1002/2015GL065911>, _eprint:
547 <https://agupubs.onlinelibrary.wiley.com/doi/pdf/10.1002/2015GL065911>.

Figure 1.

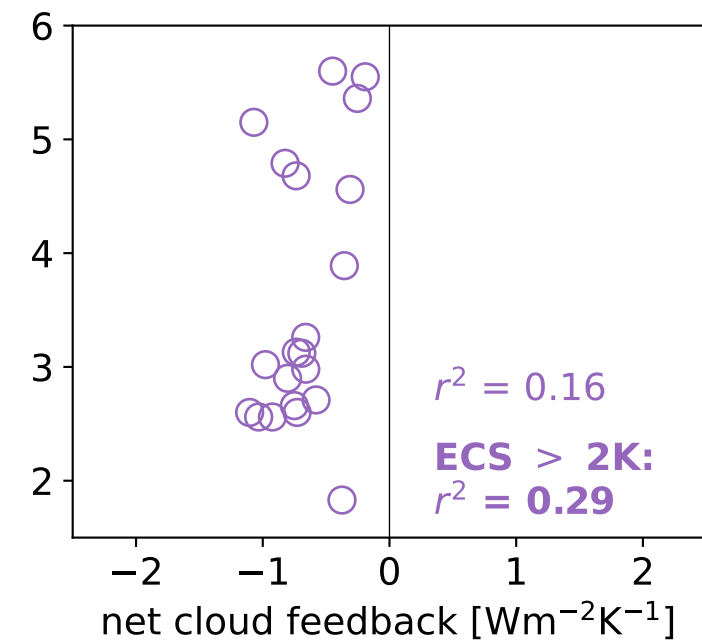
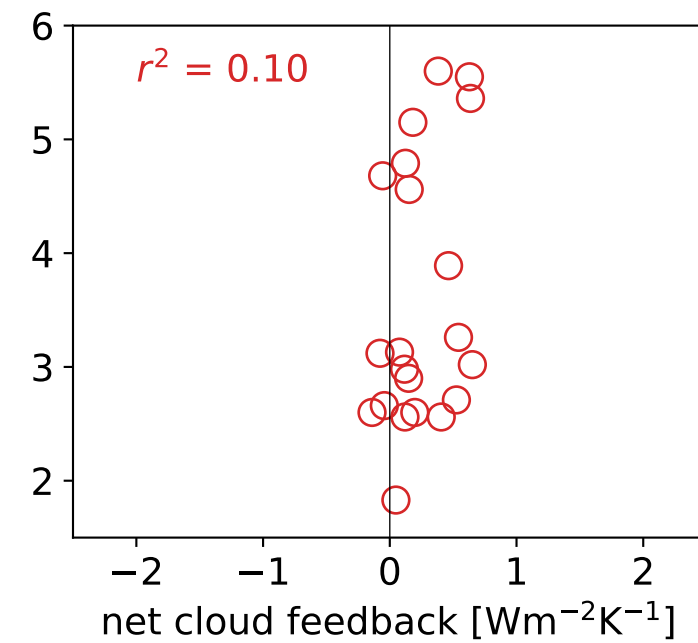
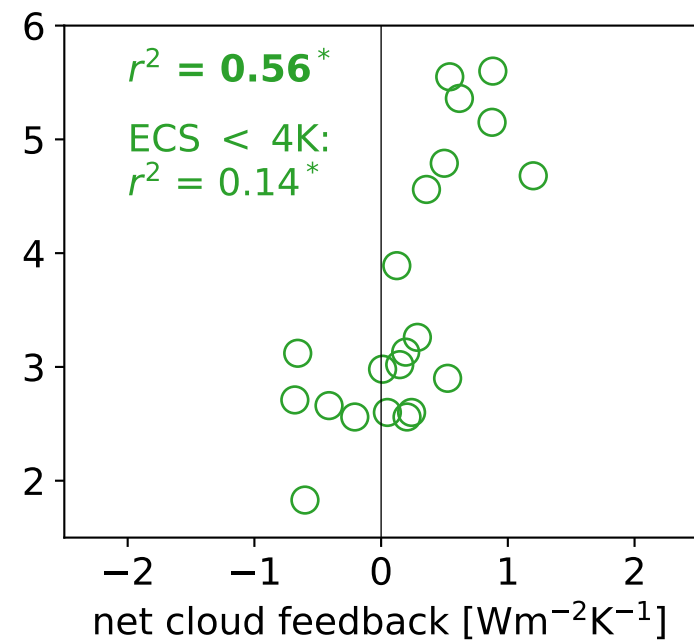
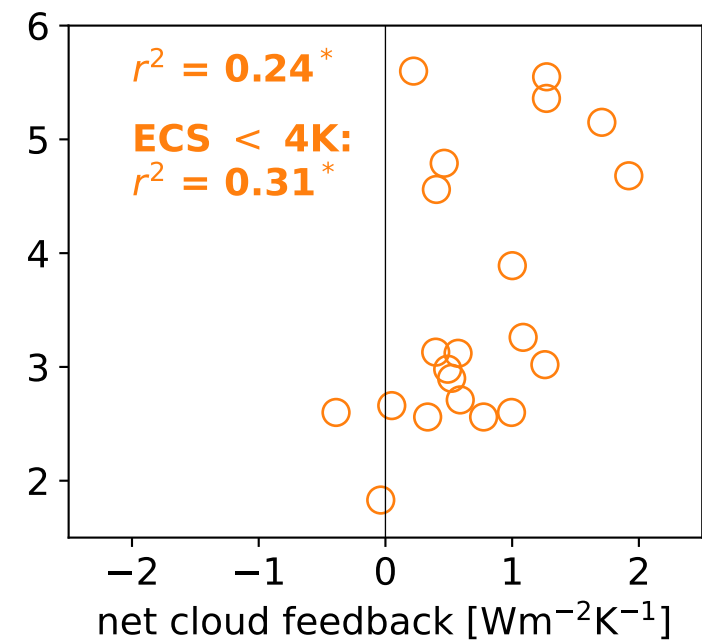
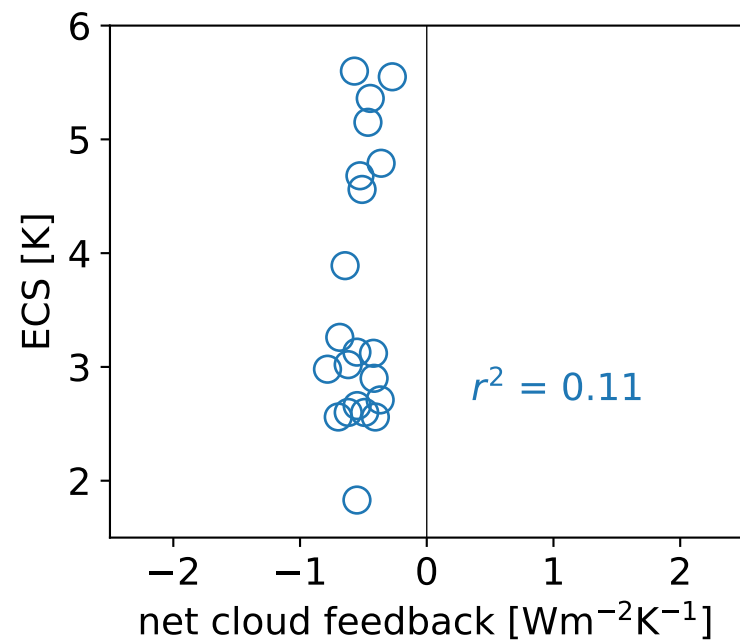
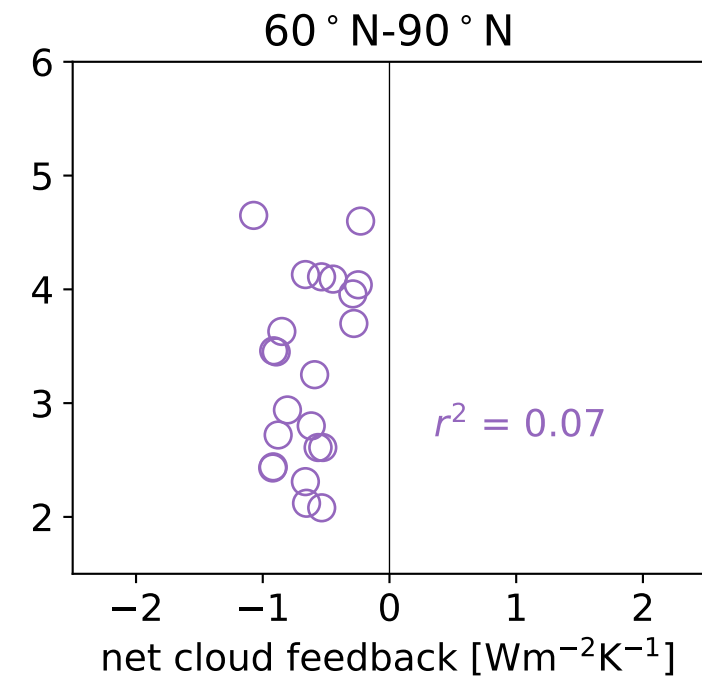
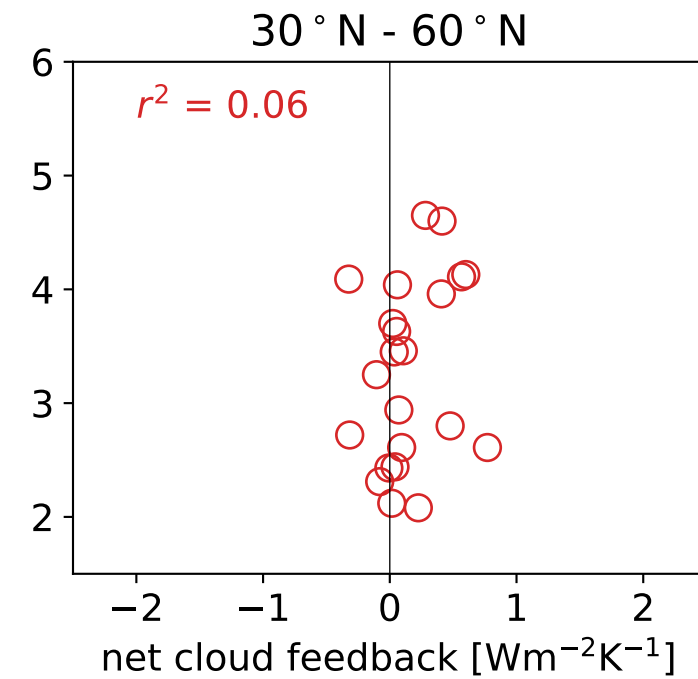
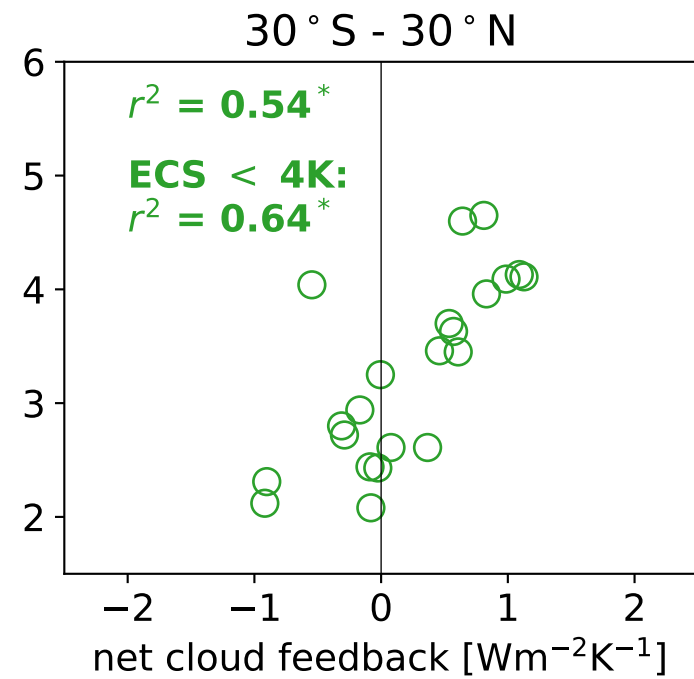
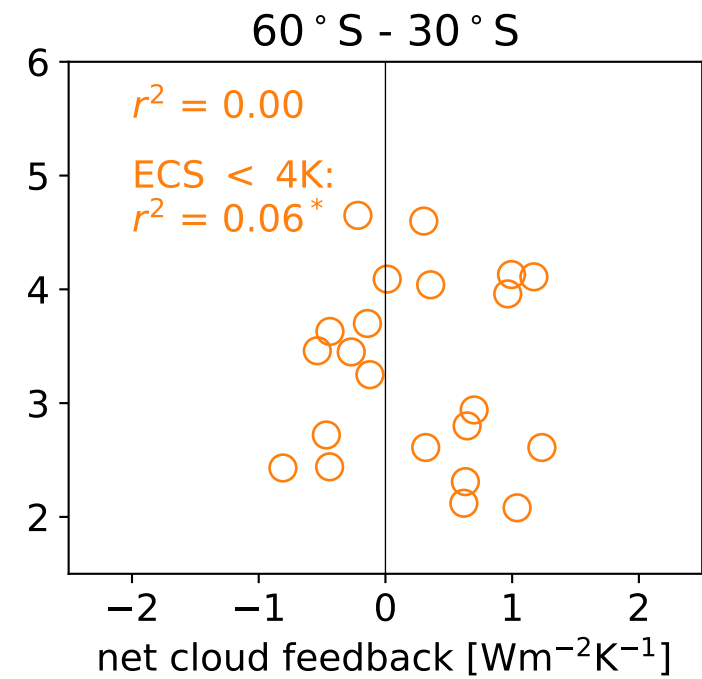
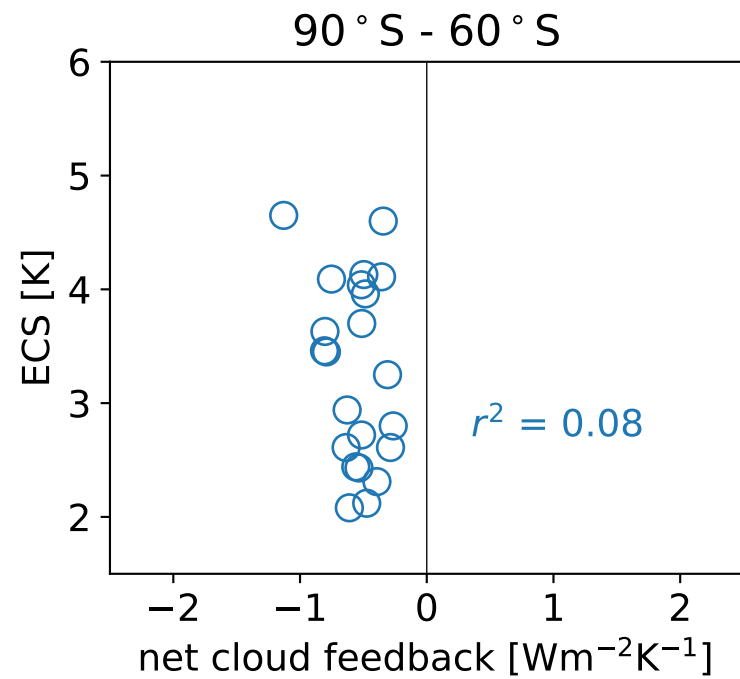


Figure 2.

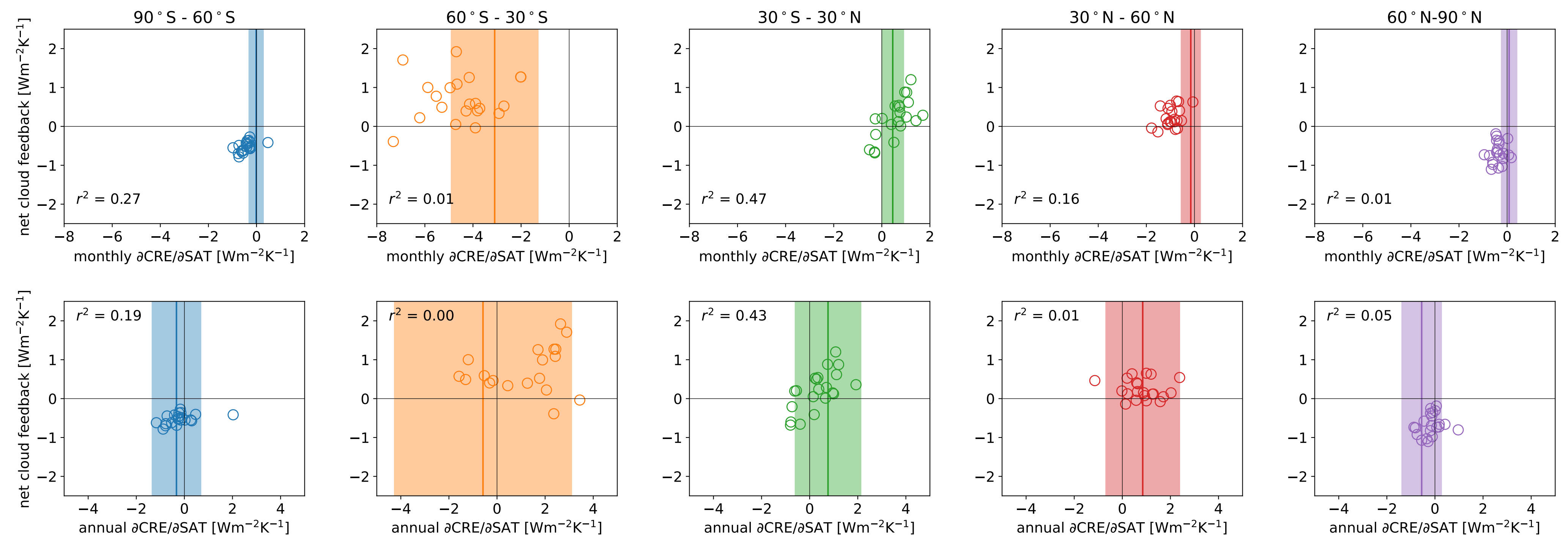


Figure 3.

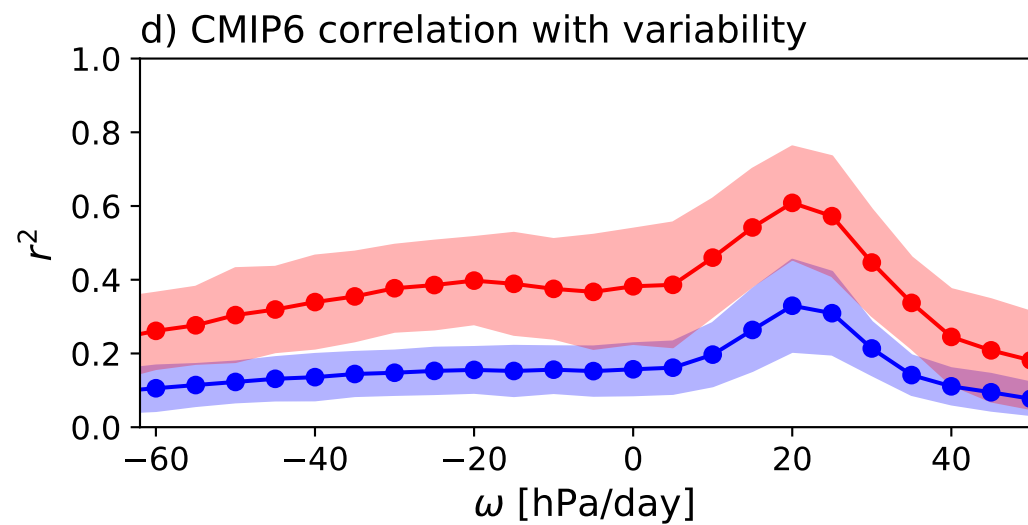
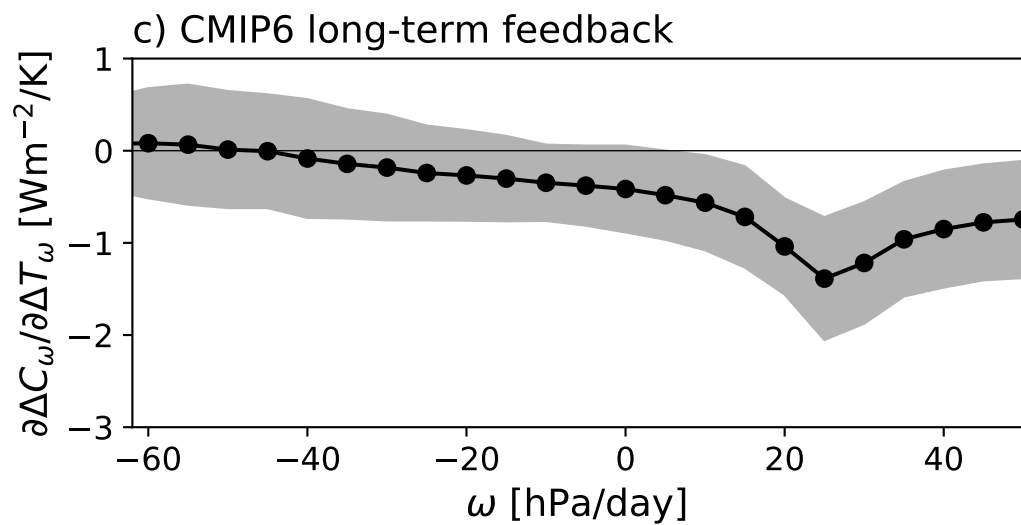
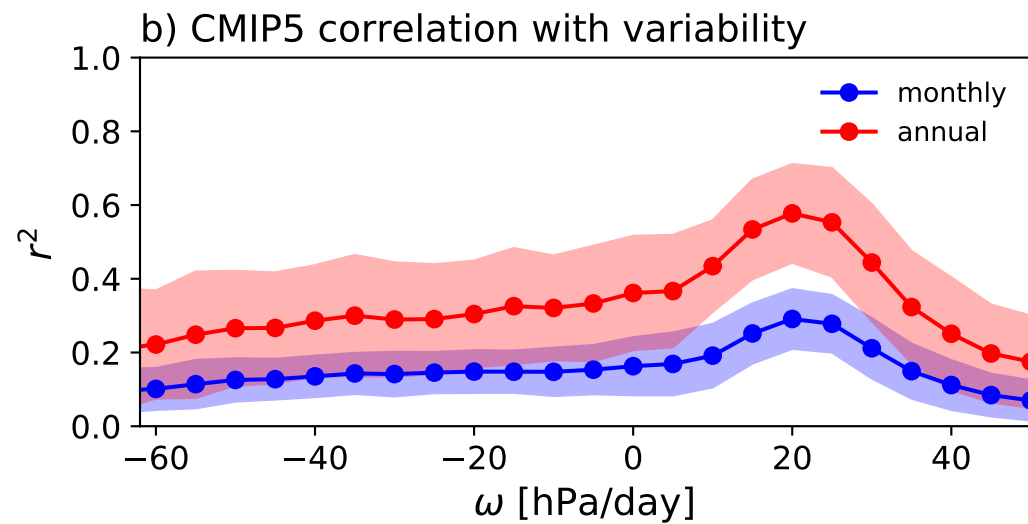
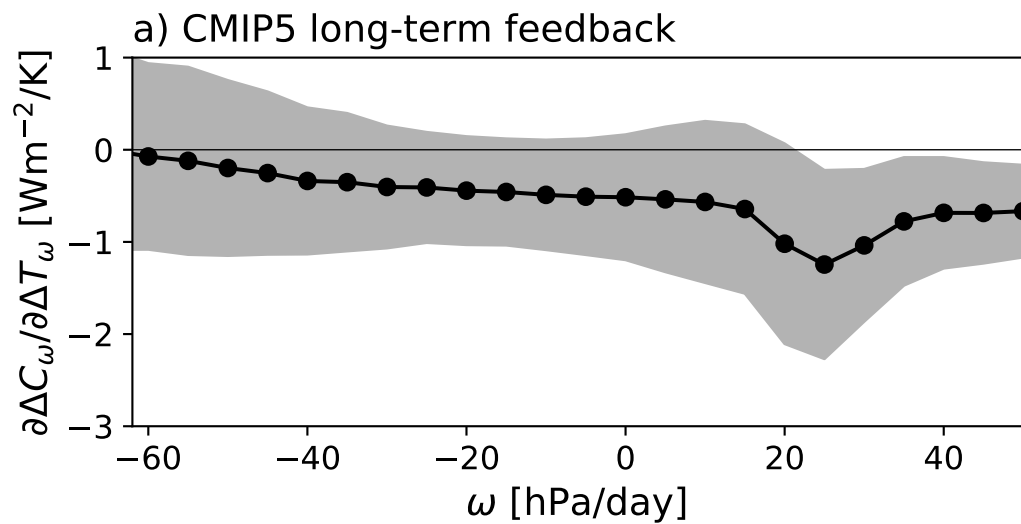


Figure 4.

